ACS SENSORS

pubs.acs.org/acssensors

Article

Development of a Genetically Encoded Sensor for Arginine

Chun Wang, Xiaoxue Zhang, Haoyu Mao, Yi Xian,* and Yi Rao*

Cite This: https://doi.org/10.1021/acssensors.4c03174

Read Online

ACCESS | Metrics & More | Article Recommendations | Supporting Information

ABSTRACT: The amino acid L-arginine (Arg) plays important roles in multiple metabolic and physiological processes, and changes in its concentration have been implicated in pathological processes. While it is important to measure Arg levels in biological systems directly and in real-time, existing Arg sensors respond to L-ornithine or L-lysine. Here we report ArgS1, a new Arg sensor. It showed a concentration-dependent increase in the ratio Ex488/405 for Arg with an apparent affinity of ~64 μM and with a dynamic range ($\Delta R/R_0$) of 3. ArgS1 responds to Arg in both the cytoplasm and the subcellular organelles. ArgS1 monitored Arg levels in MDA-MB-231 cells, a breast cancer cell line deficient in a key enzyme for Arg synthesis (arginino-succinate synthetase1, ASS1) and amenable to Arg depletion therapy. We found that Arg levels in MDA-MB-231 cells decreased after depletion of extracellular Arg with a concomitant decline in cell viability. When ASS1 was overexpressed in the cells, Arg levels increased and cell viability was also enhanced. Thus, ArgS1 is an effective tool for real-time monitoring of Arg in human cells over a dynamic range of physiological and pathological relevance.

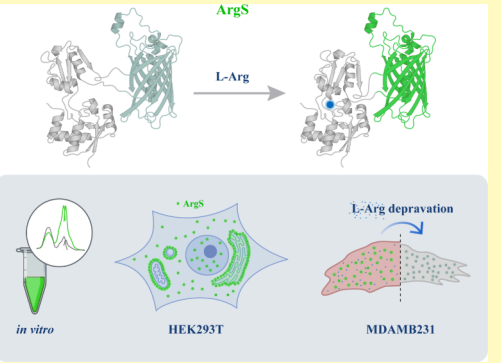

KEYWORDS: *L-arginine, fluorescent protein, fluorescent probe, biosensor, cell imaging*

In the human body, L-arginine (Arg) is a conditionally essential amino acid that is physiologically important.[1,2] The main sources of Arg include protein degradation, dietary intake, and de novo synthesis.[3] Arg synthesis involves two key enzymes: argininosuccinate synthetase (ASS), which converts L-citrulline (Cit) into argininosuccinate, and argininosuccinate lyase (ASL), which cleaves argininosuccinate into Arg.[4,5] Arg is catalyzed by nitric oxide synthases (NOS) to produce Cit and nitric oxide (NO), with Arg being the sole direct precursor of NO.[6−9] Arg participates in the urea cycle, being hydrolyzed into urea and L-ornithine (Orn) by arginases (ARGs),[10,11] which is vital for ammonia detoxification.[12] Arginine: glycine amidinotransferase (AGAT), a mitochondrial enzyme, catalyzes Arg to produce guanidinoacetate, the direct precursor of creatine.[13−15] Disorders of Arg metabolism are associated with diseases.[5,16] Arginase 1 (ARG1) deficiency leads to hyperargininemia, a rare inherited metabolic disease characterized by progressive neurological symptoms.[17] Arg is also related to disease treatment, such as erectile dysfunction,[18,19] hypertension,[20] and heart failure.[21]

Survival and growth of cancer cells require amino acids,[22−24] among which Arg is an essential component within the tumor microenvironment.[25−27] Certain types of cancer, such as breast cancer,[28] melanoma,[29] hepatocellular carcinoma,[30] acute lymphoblastic leukemia (ALL),[31] and acute myeloid leukemia (AML),[32] were deficient in ASS expression. These types of cancer depend on the uptake of extracellular Arg for survival; thus, restriction of Arg supply has been explored as a potential adjunctive therapeutic strategy in cancer treatment.[27,33] Arg-depletion of Arg from or addition of ADI-PEG20 (pegylated arginine deiminase) to culture media leads to the eradication of ASS1-deficient cancer cells in vitro.[28,34] The systemic administration of ADI or arginases to restrict Arg availability has been investigated in phase II clinical trials for oncological therapy.[35] These studies indicate that ASS1 deficiency is a prerequisite, but not a sufficient, condition for AML patients to respond to ADI-PEG20 monotherapy. Measurement of Arg is an important indicator to determine the suitability of patients for ADI-PEG20 AML treatment.

A traditional method for measuring Arg involves microdialysis of samples[36,37] and chemical analysis,[38] which lack the ability to investigate changes in intracellular distribution or to analyze Arg with the necessary spatial and temporal resolution. Optical sensors provide the possibility to non-invasively measure concentrations and variations spatially and temporally in real time. Existing genetically encoded Arg fluorescent sensors are based on Förster resonance energy transfer (FRET), which have relatively small dynamic ranges.[39−41] The largest dynamic range reported for these sensors was only about 0.6 in vitro.[40] A bigger problem lies with their specificity: these sensors responded not only to Arg but also to other

Received: November 10, 2024
Revised: December 30, 2024
Accepted: January 15, 2025

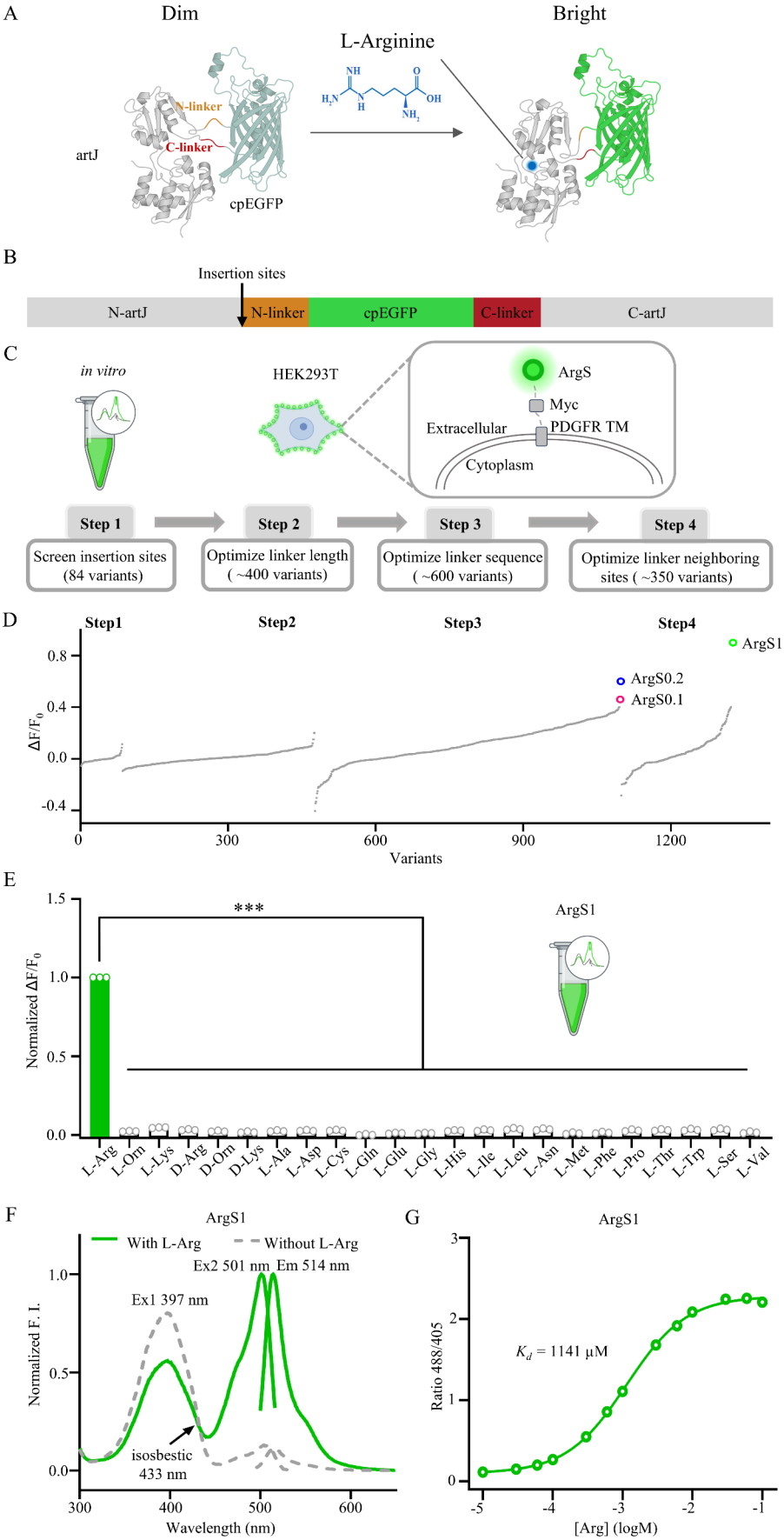

Figure 1. In vitro measurements of ArgS sensors. (A, B) Design of the ArgS sensors. The cpEGFP was integrated into the *E. coli* artJ protein via various insertion sites. We refer to the amino acid linkers between cpEGFP and artJ as the N-linker and C-linker. The model was generated by

https://doi.org/10.1021/acssensors.4c03174
ACS Sens. XXXX, XXX, XXX−XXX

Figure 1. continued

using AlphaFold2. (C) Screening procedure for ArgS sensors. Step 1 was of insertion site screening on purified proteins, steps 2−4 were on HEK293T cell membrane, steps 2 and 3 were of linker length and composition optimization, respectively, and step 4 was of linker neighboring sites optimization. (D) Screening results of ArgS sensors. ArgS0.1, ArgS0.2, and ArgS1 sensors were highlighted in magenta, blue, and green, respectively. (E) Amino acid specificity of the ArgS1 sensor. The response to 1 mM various amino acids was normalized to their response to 1 mM L-Arg. $n = 3$ per data point; data are presented as the mean ± SEM. (F) Excitation and emission spectrum of ArgS1 sensor with and without 1 mM Arg. (G) Dose−response curve of ArgS1 sensor when exposed to varying concentrations of Arg. $n = 6$ per data point; data are presented as mean ± SEM.

amino acids, such as Orn, L-lysine (Lys), L-glutamine (Gln), and L-histidine (His).[39−41] The dissociation constants (K_d) of these sensors for Arg (9.4 or 14 μM)[39,40] were not suitable for detecting physiological levels of Arg, which are typically around 100 μM in the plasma[42] and the cytoplasm.[43]

Therefore, genetically encoded Arg-specific fluorescent sensors with large dynamic ranges and suitable K_d values are needed for detection of Arg under physiological and pathological conditions.

RESULTS

Design, Optimization, and In Vitro Characterization of Arg Sensors. We engineered a genetically encoded fluorescent Arg sensor based on *Escherichia coli* (*E. coli*) artJ, a periplasmic binding protein (PBP) whose conformation changes upon Arg binding.[44−46] Similar to the design of other sensors,[47−50] we integrated a circular-permutated green fluorescent protein, cpEGFP from $GRAB_{DA2m}$[51] into artJ (Figure 1A,B). Based on the crystal structures of artJ and argT (an Arg, Lys, and Orn binding protein), the conformation of the loop regions of lobes II and the hinge regions undergo significant changes upon substrate binding,[45,46,52−56] which offered promising insertion sites for cpEGFP. First, we screened cpEGFP insertion sites on the purified protein (Figure 1C). The linkers between artJ and cpEGFP were either flexible (Gly-Gly) or rigid (Pro-Pro). Based on the results of the first screening, we selected sensors with maximum dynamic ranges greater than 0.1 (Figure 1D). Considering the time-consuming nature of protein-purification-based screening methods and the fact that sensors that respond in vitro may not exhibit the same responsiveness in a cellular environment, we switched to conduct screening using HEK293T cells. By fusing those sensors with a membrane-targeting sequence from iSeroSnFR.[57] We targeted the sensors to the cell membrane of human embryonic kidney 293T (HEK293T) cells to optimize the length and amino acid composition of the linkers, thereby minimizing the influence of intracellular Arg on the sensor's response. We found that the sensors exhibiting good responses on the HEK293T cell membrane had response values of 0.4 and 0.6, which we designated as ArgS0.1 and ArgS0.2, respectively (Figure 1C,D and Supporting Information Figure S1C). Subsequently, we optimized the linker neighboring sites and found that the best responding sensor had a response of 0.9, which we have named ArgS1 (Figure 1D, Figure S1C). In summary, screening through more than 1200 different variants, we identified three sensors, named ArgS0.1, ArgS0.2, and ArgS1 (Figure 1D).

We expressed each of these three sensors in *E. coli* and purified them. Then we tested the specificity of the ArgS sensors for various amino acids and found that all three ArgS sensors responded specifically to L-Arg, without reacting to either the L- or D-forms of other amino acids (Figure 1E, Figure S2A,B). All three ArgS sensors exhibited ratiometric characteristics, with two excitation peaks near 400 and 500 nm and one emission peak near 515 nm. Upon binding with 1 mM Arg, the 400 nm excitation peaks of the three ArgS sensors decreased, whereas the 500 nm excitation peaks increased (Figure 1F, Figure S2C,D). We also measured the Arg binding affinities of ArgS0.1, ArgS0.2, and ArgS1, which showed K_d values of 73, 367, and 1141 μM, respectively. The peak changes in fluorescence ($\Delta R/R_0$) were 1.9, 4.6, and 19, respectively (Figure 1G, Figure S2E,F). Besides, we evaluated the specificity of the ArgS sensors toward Arg-related metabolites. ArgS0.1 exhibited detectable responses to agmatine, Cit, and argininosuccinic acid, whereas ArgS0.2 and ArgS1 responded to Cit and argininosuccinic acid (Figure S3A,D,G). For Cit binding, ArgS0.1, ArgS0.2 and ArgS1 showed K_d of 312 μM, 1162 μM and 2912 μM, respectively, with peak fluorescence changes approximately half of those observed for Arg Figure S3B,E,H). In the case of argininosuccinic acid binding, the K_d values exceeded 300 μM for all sensors (Figure S3C,F,G). To mitigate potential interference from Arg-related metabolites during Arg measurements using ArgS sensors, we quantified the intracellular concentrations of these metabolites in both HEK293T and MDA-MB-231 cells by LC-MS. In both cell lines, the concentrations of Cit and argininosuccinic acid were below 5 μM (Cit: 1.290 μM in HEK293T and 3.920 μM in MDA-MB-231 cells; argininosuccinic acid: 1.556 μM in HEK293T and 4.156 μM in MDA-MB-231 cells), which are below the detection thresholds of the ArgS sensors (Figure S3J). Therefore, when quantifying Arg levels in HEK293T or MDA-MB-231 cells, the potential interfer-ence from Cit or argininosuccinic acid can be considered negligible. In addition, based on the crystal structure of *Geobacillus stearothermophilus* artJ,[45] we developed three mutant versions of the ArgS1 sensors. Among them, the double-point mutant version ArgS1-F51L E114L exhibits almost no response to Arg (Figure S4C). Therefore, this version of the sensor, ArgS1-F51L E114L, is named ArgS1-C and serves as a control for subsequent experiments. To investigate pH dependence, we tested ArgS1 and ArgS1-C across a pH range of 4−9. ArgS1 exhibited optimal response to Arg at pH values between 7 and 8 (Figure S4A), while the apo forms of both ArgS1 and ArgS1-C displayed similar pH-dependent behavior across the tested range (Figure S4B).

Detection of Arg Changes in the Cytoplasm and Subcellular Organelles of HEK293T Cells by Arg Sensors. To investigate whether Arg sensors could detect Arg in mammalian cells, we expressed ArgS0.1, ArgS0.2, and ArgS1 in the cytoplasm of HEK293T cells (Figure 2A). Arg transporters SLC7A1[58] and SLC7A2[59] were highly expressed in HEK293T cells (Figure S5A). After the extracellular concentration of Arg was raised to 1 mM Arg, we immediately observed a decrease of fluorescence intensity at 405 nm and an increase at 488 nm for the ArgS1, ArgS0.1, and ArgS0.2 (Figure 2B, Figure S6A). This indicates that all three sensors,

https://doi.org/10.1021/acssensors.4c03174
ACS Sens. XXXX, XXX, XXX−XXX

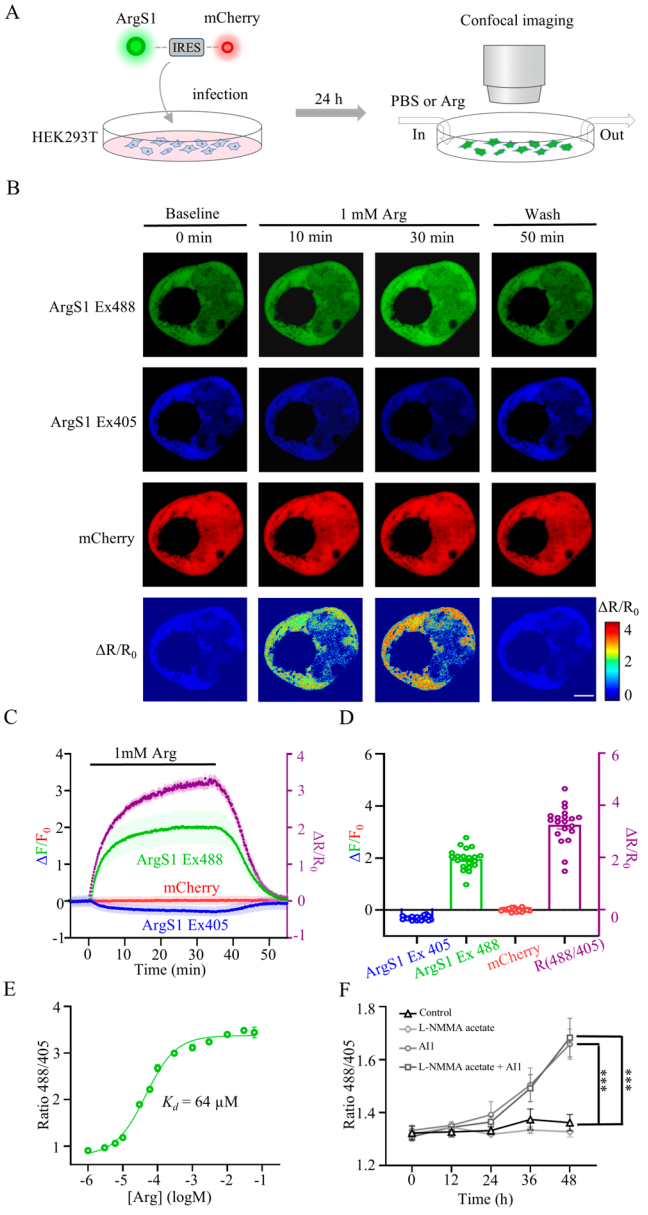

Figure 2. Response of the ArgS1 sensor in HEK293T cytoplasm to Arg concentration changes. (A) Schematic view of ArgS sensors imaging in HEK293T cytoplasm. In the cytoplasm of HEK293T cells, ArgS sensors fused with an IRES-mCherry sequence at the C-terminus were transfected and subsequently imaged using a confocal microscope under various solvent perfusion conditions. (B) Representative images showing the response of the ArgS1 sensor in the cytoplasm of HEK293T cells to changes in PBS or 1 mM Arg over different time intervals (0, 10, 30, and 50 min). The fluorescence of the ArgS1 sensor was visible in two channels: ArgS1 Ex488 (excitation at 488 nm) appeared green, while ArgS1 Ex405 (excitation at 405 nm) appeared blue. Additionally, mCherry, fused to the C-terminus of ArgS sensors via an IRES sequence, was represented in the mCherry channels in red. The change in the Ex488/Ex405 ratio of the ArgS1 sensor was further visualized in the $\Delta R/R_0$ channels. Scale bar: 10 μm. (C) Average traces of the fluorescence response of ArgS1 measured in PBS or 1 mM Arg. We perfused 1 mM Arg into HEK293T cells expressing ArgS1 sensor at 0 min, and switched to PBS buffer at 35 min. $\Delta F/F_0$ of the ArgS1 sensor under a 405 nm excitation wavelength that was represented in blue, while $\Delta F/F_0$ under a 488 nm wavelength was in green. The $\Delta F/F_0$ of mCherry was represented in red. Purple represents $\Delta R/R_0$ (the right Y-axis). n = 20 cells; data are presented as mean ± SEM. (D) Maximum response of ArgS1 sensor to Arg perfusion. n = 20 cells; data are presented as mean ± SEM. (E) Dose dependent curve with corresponding K_d values of ArgS1 sensor in the HEK293T cytoplasm. n = 600 cells from 6 wells; data are presented as mean ± SEM. (F) Pharmacological alteration of Arg concentration in HEK293T cells. The ratio of 488/405 of the ArgS1 sensor, pre- and post-incubation with 500 μM inhibitors for a durations of 12, 24, 36, and 48 h, respectively. The control group was represented in black equilateral triangle, the L-NMMA acetate alone group was represented in gray rhombus, the AI1 alone group was represented in gray circle, and the L-NMMA and AI1 combination group was represented in dark gray square. n = 600 cells from 6 wells; data are presented as mean ± SEM.

ArgS1, ArgS0.1, and ArgS0.2, responded to increased Arg, with maximum dynamic ranges of 3.3, 0.3, and 1.1, respectively (Figure 2D, Figure S6D,E). After the ArgS sensors reached their peak dynamic ranges, we switched the perfusion fluid back to phosphate-buffered saline (PBS). An immediate increase of fluorescence intensity at 405 nm and a decrease at 488 nm were observed for three ArgS sensors, with their responses returning to baseline values (Figure 2 C, Figure S6B,C). To perform an in situ titration to measure the Arg binding affinity of ArgS1 in the cytoplasm of HEK293T cells, cell membranes were permeabilized with digitonin, and various concentrations (1 to ∼60000 μM) of Arg were added to the cells (Figure S5B). The average response from cells expressing ArgS1 versus the concentration of Arg was plotted to provide an in situ calibration curve. So, we measured the Arg binding affinity of ArgS1 in the cytoplasm of HEK293T cells, which showed a K_d of 64 μM (Figure 2E). Additionally, to minimize nonspecific fluorescent signal changes, we expressed a nonbinding control, ArgS1-C, in HEK293T cells. As shown in Figure S5D, the ArgS1-C exhibited no response to 1 mM Arg perfusion.

To determine whether Arg sensors could detect changes in Arg caused by pharmacological interventions in HEK293T cells, we expressed ArgS1 in these cells. We utilized arginase I and II inhibitor (Arginase Inhibitor 1, AI1)[60] and an NOS inhibitor L-NMMA[61−65] to manipulate Arg levels. As demonstrated in Figure 2F, an increase in intracellular Arg levels induced by AI1 or the combined application of AI1 and L-NMMA was detected using ArgS1; however, L-NMMA alone did not induce a similar response. These results indicate that the arginase pathway is more important in Arg degradation than the NOS pathway in HEK293T cells. This conclusion is consistent with our transcriptome sequencing results. Within HEK293T cells, the expression level of ARG2 is the highest, while the expression levels of ARG1 and NOS2 are very low, and NOS1 is not expressed (Figure S5C). Thus, the ArgS1 sensor effectively monitored the pharmacologically altered Arg concentrations in HEK293T cells.

To further investigate whether Arg sensors could respond to Arg in subcellular organelles, we targeted ArgS1(Figure 3) and ArgS0.1 (Figure S7) to different organelles. We fused ArgS1 and ArgS0.1 with an N-terminal 30 amino acid leader sequence from AKAP1,[66] the ER-targeting motif of p450,[67] a LAMP1-derived sequence[68] or a nuclear localization signal[69] for localization to the mitochondrial cytoplasm side (Mito-ArgS1 and Mito-ArgS0.1), the ER cytoplasm side (ER-ArgS1 and ER-ArgS0.1), the lysosome (Lyso-ArgS1 and Lyso-ArgS0.1), or nucleus (Nuc-ArgS1 and Nuc-ArgS0.1), respectively (Figure

https://doi.org/10.1021/acssensors.4c03174
ACS Sens. XXXX, XXX, XXX−XXX

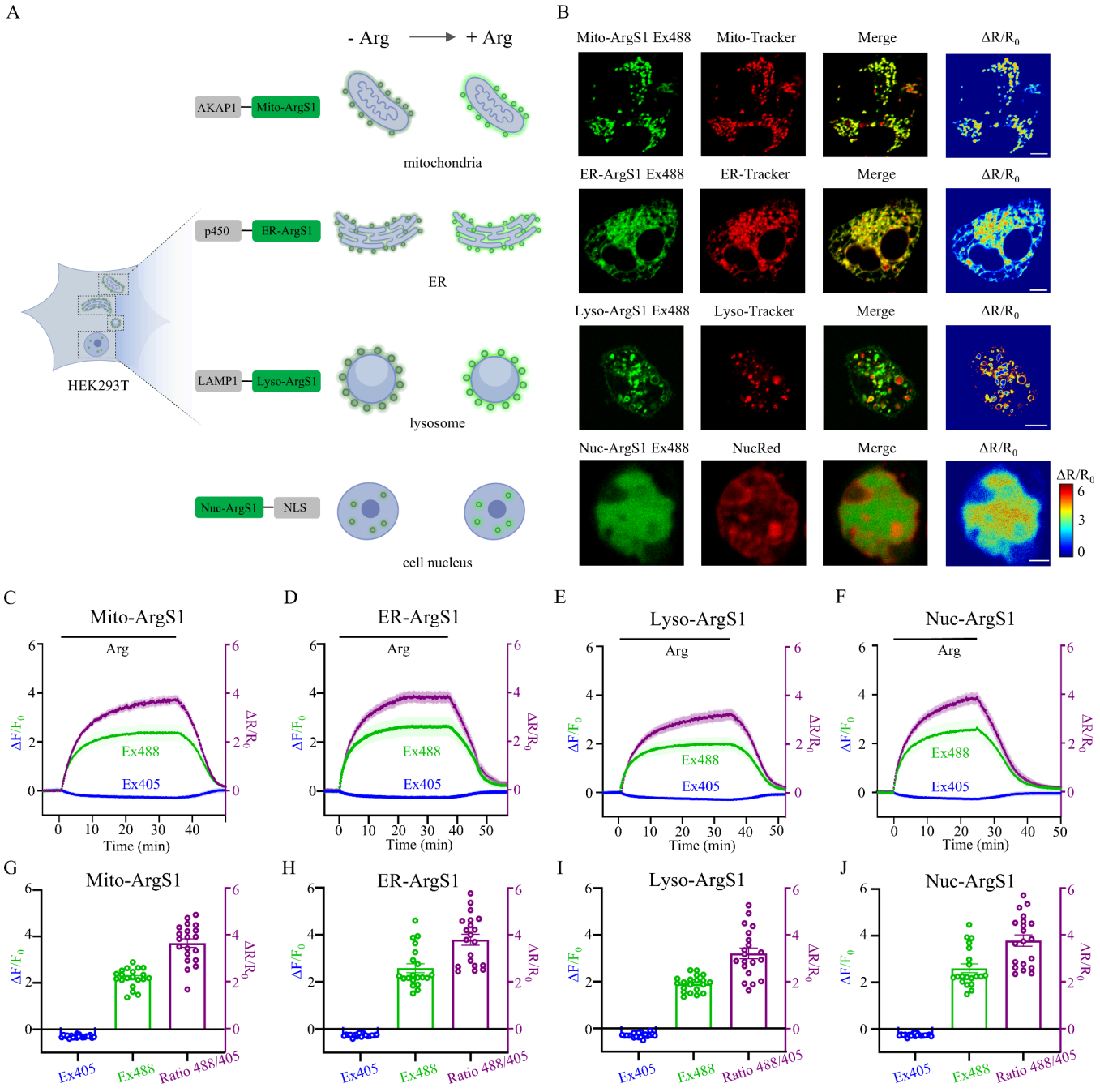

Figure 3. Response of the ArgS1 sensor in HEK293T organelles to 1 mM Arg perfusion. (A) Schematic view of ArgS1 sensor expressing in various organelles: mitochondria, ER, lysosome, and nucleus. (B) Images of ArgS1 sensor localized in various cellular compartments: on the cytoplasmic side of the mitochondrial outer membrane (Mito-ArgS1), on the cytoplasmic side of the ER membrane (ER-ArgS1), on the cytoplasmic side of the lysosomal membrane (Lyso-ArgS1), and in the nucleus (Nuc-ArgS1). The fluorescence of the ArgS1 sensor was represented in the ArgS1 channels in green. Organelle-specific markers, Mito-Tracker for mitochondria, ER-Tracker for ER, Lyso-Tracker for lysosomes, and NucRed for the nucleus, were represented in the organelle marker channels in red. The combined image of ArgS1 sensor fluorescence and organelle marker fluorescence were displayed in the Merge channels. The response of the ArgS1 sensor to Arg perfusion was represented in $\Delta R/R_0$ channels. Scale bar: 5 μm. (C–F) Average traces of the fluorescence response of ArgS1 localized in various cellular compartments measured in PBS or 1 mM Arg. We perfused 1 mM Arg into HEK293T cells expressing the Mito-ArgS1, ER-ArgS1, Lyso-ArgS1, and Nuc-ArgS1 sensors at 0 min and followed it with PBS buffer once the maximum response was achieved, respectively. The $\Delta F/F_0$ of the ArgS1 sensor at an excitation wavelength of 405 nm was represented in blue, while the $\Delta F/F_0$ at 488 nm was in green. The $\Delta R/R_0$ was represented in purple. n = 20 cells; data are presented as mean ± SEM. (G–J) Maximum response of Mito-ArgS1, ER-ArgS1, Lyso-ArgS1, and Nuc-ArgS1 to 1 mM Arg perfusion. n = 20 cells; data are presented as mean ± SEM.

3A). To assess the localization of ArgS1 in the mitochondria, ER, lysosome, and nucleus, we used Mito-Tracker, ER-Tracker, Lyso-Tracker, and NucRed as controls. ArgS sensors were found to be highly colocalized with corresponding organelle markers (Figure 3B, Figure S7A). When 1 mM Arg was perfused into the media culturing HEK293T cells, ArgS sensors localized in organelles also responded to changes in Arg levels (Figure 3C–F, Figure S7B–E). The maximum

https://doi.org/10.1021/acssensors.4c03174
ACS Sens. XXXX, XXX, XXX−XXX

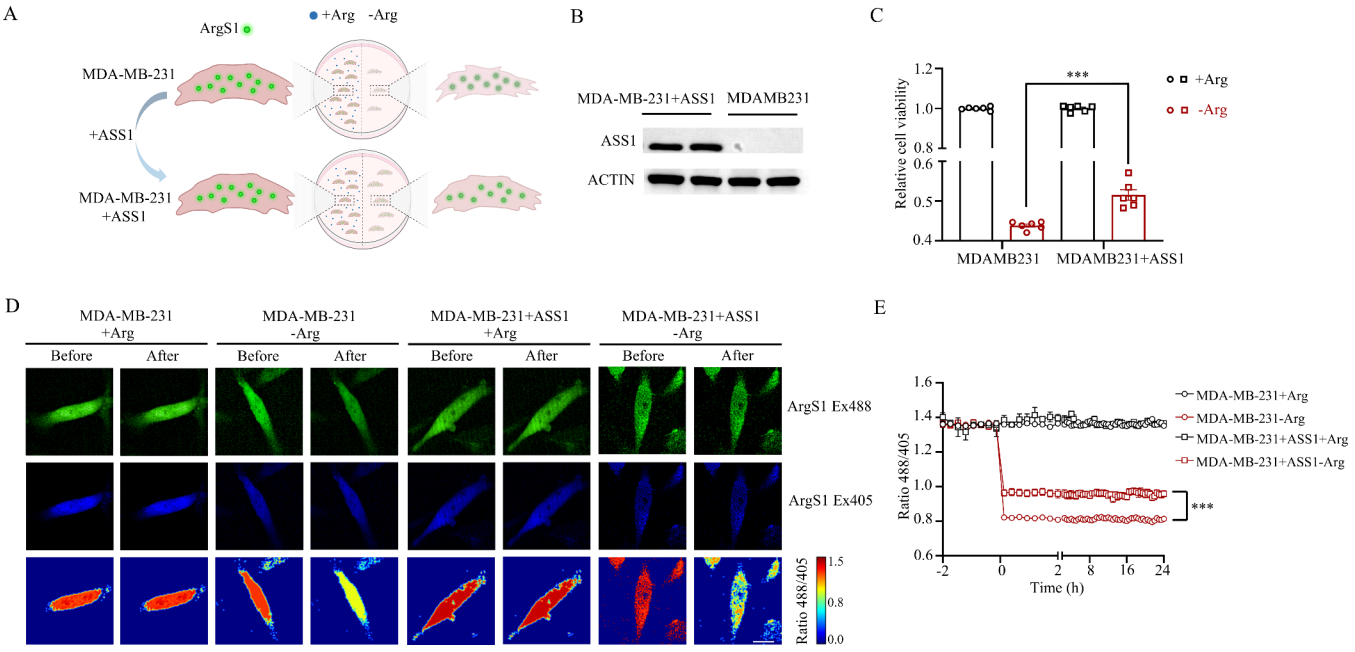

Figure 4. Imaging Arg in MDA-MB-231 cells. (A) Schematic view of ArgS1 sensor expressed in MDA-MB-231 cells with and without Arg starvation. (B) Expression levels of ASS1 in MDA-MB-231 cells and ASS1 overexpressed MDA-MB-231 cells. (C) Cell viability of MDA-MB-231 cells (in circle) and ASS1 overexpressed cells (in square), following Arg starvation (deep red) or complete DMEM control for 24 h (black). Both cell viabilities of the Arg starved group were normalized to the complete DMEM control group. n = 600 cells from 6 wells; data are presented as mean ± SEM. (D) Fluorescence intensity and response change of the ArgS1 sensors in MDA-MB-231 cells and ASS1 overexpressing MDA-MB-231 cells was imaged before and after 30 min of Arg starvation. Scale bar, 10 μm. (E) Ratio of 488/405 change of the ArgS1 sensors in MDA-MB-231 cells and ASS1 overexpressing MDA-MB-231 cells was imaged every 15 min before 2 h and after 24 h of Arg starvation. n = 600 cells from 6 wells; data are presented as mean ± SEM.

dynamic ranges of Mito-ArgS1, ER-ArgS1, Lyso-ArgS1, and Nuc-ArgS1 sensors were 3.7, 3.8, 3.2, and 3.8 (Figure 3G–J), respectively, and the maximum dynamic ranges of Mito-ArgS0.1, ER-ArgS0.1, Lyso-ArgS0.1, and Nuc-ArgS0.1 sensors were 0.5, 0.5, 0.4, and 0.6 (Figure S7F–I), respectively. These results indicate that the response of ArgS sensors in the regions near the mitochondria, ER, and lysosomes, as well as within the nucleus, were similar. Thus, we successfully developed ArgS sensors capable of monitoring Arg in the cytoplasm and subcellular organelles of mammalian cells.

Decreased Intracellular Arg Levels in Cancer Cells Caused by Deprivation of Extracellular Arg. Arg starvation is being explored as a potential treatment strategy for ASS1-deficient cancers[28,70] (Figure 4A). It has been reported that the breast cancer cell line MDA-MB-231 does not express ASS1[28] (Figure 4B). Here we first confirmed the effect of Arg deprivation on cell viability. The viability of MDA-MB-231 cells decreased after 24 h of Arg deprivation (Figure 4C), consistent with previous reports.[28] Besides, overexpression of ASS1 rescued the vulnerability of MDA-MB-231 cells to Arg starvation (Figure 4B,C). To observe intracellular Arg levels, we developed MDA-MB-231 cell lines that stably expressed ArgS1 in MDA-MB-231 cells (Figure 4A). We found that after Arg deprivation, both the ratio of 488/405 of the ArgS1 sensor and the decay rate of the ratio significantly decreased, indicating that the intracellular Arg level in MDA-MB-231 cells was significantly lower than in the control group (Figure 4D,E, Figure S8B). Besides, after Arg deprivation, both the ratio of 488/405 of the ASS1 overexpressed group was higher than the ASS1-deficient group, indicating the Arg level was rescued via ASS1 overexpression (Figure 4D,E). Additionally, to further minimize nonspecific fluorescent signal changes, we expressed ArgS1-C in MDA-MB-231 cells. As shown in Figure S8A, the ArgS1-C also exhibited no response to 1 mM Arg perfusion. Therefore, Arg levels can be monitored in cancer cells using an ArgS1 sensor.

DISCUSSION

In our effort to compare ArgS sensors with other Arg sensors, we have compiled the characteristics of various Arg sensors in Table S1. For example, the QBP/citrine/ECFP sensor, based on gln H, exhibited a K_d of 2.1 mM for Arg and a dynamic range of 0.3.[39] Additionally, the FLIP-cpargT194 sensor, based on argT, demonstrated a K_d of 48 μM for Arg and a dynamic range of 0.5.[40] However, these sensors were not exclusively specific to Arg: QBP/Citrine/ECFP also responded to Orn, while FLIP-cpargT194 was responsive to both Orn and Lys.[39,40] In contrast, FLIP-cpartJ185 and FLIPR sensors were specific to Arg, with K_d values of 9.4 and 14 μM and dynamic ranges of 0.5 and 0.3, respectively.[40,41] Due to the limited response and specificity of these sensors toward Arg, they were not ideal for detecting changes in Arg concentration within mammalian cells. By comparison, the ArgS sensors—ArgS0.1, ArgS0.2, and ArgS1—have K_d values of 73, 367, and 1141 μM, respectively, with peak fluorescence changes ($\Delta R/R_0$) of 1.9, 4.6, and 19, respectively. These responses are superior to those of previous Arg sensors, and ArgS sensors specifically respond to Arg without cross-reacting with other amino acids. Recently, a genetically encoded sensor named STAR was reported, which specifically responds to Arg and is capable of monitoring Arg dynamics both in vitro and in vivo.[71] Compared to STAR, ArgS1 exhibited a slightly larger fluorescence response ($\Delta R/R_0$: 19 vs ~16 in vitro). However, unlike ArgS1, STAR does

https://doi.org/10.1021/acssensors.4c03174
ACS Sens. XXXX, XXX, XXX−XXX

not exhibit ratiometric characteristics, necessitating additional controls to account for variations in sensor expression levels.

To enhance the maximum response of ArgS sensors, we screened various linker lengths and compositions. It was observed that two or three amino acids at the N-terminal linkers and two at C-terminal linkers yielded a greater response, with Gly being preferred as the first amino acid in the N-terminal linker. Additionally, during step 4 of the screening process, the amino acid residue adjacent to the N-terminal linker was tested. For example, replacing this residue with Ile significantly improved the response, leading to the development of ArgS1. Although we screened over 1200 candidates, further improvement is possible by expanding the screening to include additional neighboring linker sites.

Specifically, ArgS1 in the cytoplasm of HEK293T cells exhibited a K_d value of 64 μM, which is higher than the value measured in vitro. Similarly, the affinity of iGluSnFR sensors in HEK293T cells or cultured hippocampal neurons was higher than that observed in vitro.[47,49,72] This discrepancy may be due to differences in the protein's exposure to various environments and detection systems, or it could be the result of cofactors in the cellular environment that enhance Arg binding. However, even after adding cell lysate to the detection system during in vitro experiments, the measured K_d remained in the millimolar range, suggesting the need for further investigation. Therefore, to accurately quantify Arg levels across different environments, K_d should be measured under a variety of experimental conditions to account for these factors. Moreover, ArgS1 exhibited detectable responses to Cit and argininosuccinic acid. When measuring Arg levels in di-verse biological environments, it is essential to verify that the concentrations of Cit and argininosuccinic acid remain below the detection threshold of the ArgS1 sensor.

Regarding the dynamics of ArgS sensors in different subcellular locations, the timing of arginine perfusion for Nuc-ArgS1 and ER-ArgS1 was shorter compared to other locations, which may reflect subcellular differences in arginine metabolism (Figure 3C−F). Additionally, we attempted to determine the basal Arg concentrations at each subcellular location; however, we were uncertain whether the initial ratio before perfusion accurately reflected the basal concentration, as the apo-form ratio may vary across subcellular compartments. Furthermore, depleting Arg at each subcellular location to obtain the apo-form of the ArgS sensors proved challenging. Therefore, we chose not to quantify Arg concentrations at subcellular locations until a more reliable method for obtaining the apo-form of the ArgS sensors in these compartments becomes available.

Arg plays a crucial role in both physiological and pathological processes; however, many of its functions remain poorly understood. For example, the mechanisms of Arg transport between astrocytes and neurons are still unknown, and its role as a signaling molecule is not well-defined. Moreover, changes in Arg concentration could be monitored alongside other molecules, such as Ca^{2+}, cAMP, and Glu, using complementary fluorescent sensors. We hope that our ArgS sensors will contribute to elucidating the mechanisms of Arg metabolism and provide deeper insights into its physiological and pathological roles.

CONCLUSIONS

In summary, ArgS1 enables real-time detection of Arg level changes in various mammalian cells, providing valuable insights for both basic research and clinical applications. This represents the first genetically encoded fluorescent sensor capable of dynamically monitoring the Arg concentration changes within mammalian cells. Furthermore, ArgS1 exhibits a dynamic responsiveness to Arg within subcellular organelles and has been successfully employed to monitor Arg levels in MDA-MB-231 breast cancer cells.

ASSOCIATED CONTENT

Supporting Information

The Supporting Information is available free of charge at https://pubs.acs.org/doi/10.1021/acssensors.4c03174.

Materials and methods; sensor screening procedure; sensor in vitro measurements; Characterization of ArgS sensor responses to Arg-related metabolites; pH dependences; transcriptome sequencing results and response of perfusion in cells.; concentration changes responses; sensor response to Arg perfusion; ArgS1-C to Arg deprivation and perfusion response; and sensor decay rate during Arg deprivation; various Arg sensors characteristics (PDF)

AUTHOR INFORMATION

Corresponding Authors

Yi Xian − *Changping Laboratory, Chinese Institute of Brain Research, Beijing, Beijing 102206, China; Research Unit of Medical Neurobiology, Chinese Academy of Medical Sciences, Beijing 102206, China; Laboratory of Neurochemical Biology, Department of Chemical Biology, College of Chemistry and Molecular Engineering, Peking-Tsinghua Center for Life Sciences, PKU-IDG/McGovern Institute for Brain Research, School of Life Sciences, School of Pharmaceutical Sciences and Peking University, Beijing 100871, China;* orcid.org/0000-0002-4031-0332; Email: xianyistevenx@outlook.com

Yi Rao − *School of Basic Medical Sciences, Capital Medical University, Beijing 100069, China; Chinese Institute for Brain Research, Beijing 102206, China; Changping Laboratory, Chinese Institute of Brain Research, Beijing, Beijing 102206, China; Research Unit of Medical Neurobiology, Chinese Academy of Medical Sciences, Beijing 102206, China; Laboratory of Neurochemical Biology, Department of Chemical Biology, College of Chemistry and Molecular Engineering, Peking-Tsinghua Center for Life Sciences, PKU-IDG/McGovern Institute for Brain Research, School of Life Sciences, School of Pharmaceutical Sciences and Peking University, Beijing 100871, China; Chinese Institutes for Medical Research, Beijing (CIMR, Beijing), Capital Medical University, Beijing 100069, China*; Email: yrao@pku.edu.cn

Authors

Chun Wang − *School of Basic Medical Sciences, Capital Medical University, Beijing 100069, China; Chinese Institute for Brain Research, Beijing 102206, China; Changping Laboratory, Chinese Institute of Brain Research, Beijing, Beijing 102206, China; Research Unit of Medical Neurobiology, Chinese Academy of Medical Sciences, Beijing 102206, China*

Xiaoxue Zhang − *Changping Laboratory, Chinese Institute of Brain Research, Beijing, Beijing 102206, China; Research*

https://doi.org/10.1021/acssensors.4c03174
ACS Sens. XXXX, XXX, XXX−XXX

Unit of Medical Neurobiology, Chinese Academy of Medical Sciences, Beijing 102206, China

Haoyu Mao − *Changping Laboratory, Chinese Institute of Brain Research, Beijing, Beijing 102206, China; Research Unit of Medical Neurobiology, Chinese Academy of Medical Sciences, Beijing 102206, China; Laboratory of Neurochemical Biology, Department of Chemical Biology, College of Chemistry and Molecular Engineering, Peking-Tsinghua Center for Life Sciences, PKU-IDG/McGovern Institute for Brain Research, School of Life Sciences, School of Pharmaceutical Sciences and Peking University, Beijing 100871, China*

Complete contact information is available at: https://pubs.acs.org/10.1021/acssensors.4c03174

Notes

The authors declare no competing financial interest.

■ ACKNOWLEDGMENTS

We thank Prof. Yulong Li for offering the $GRAB_{DA2m}$ plasmid. We thank National Center for Protein Sciences at Peking University in Beijing, China for assistance with Operetta high-content imaging. We thank the Biological Mass Spectrometry Center, Chinese Institute for Brain Research, Beijing, China and Ms. Xiaoqian Yu for the assistance with LC-MS analyses.

■ REFERENCES

(1) Albaugh, V. L.; Stewart, M. K.; Barbul, A. Chapter 27 - Cellular and Physiological Effects of Arginine in Seniors. In *Nutrition and Functional Foods for Healthy Aging*; Watson, R. R., Ed.; Academic Press, 2017; pp 317−336. DOI: 10.1016/B978-0-12-805376-8.00027-7.

(2) Albanese, A. A. The Amino Acid Requirements of Man. In *Advances in Protein Chemistry*, Vol. 3; Anson, M. L., Edsall, J. T., Eds.; Academic Press, 1947; pp 227−268.

(3) Albaugh, V. L.; Barbul, A. Arginine. In *Reference Module in Life Sciences*; Elsevier, 2017.

(4) Jackson, M. J.; Beaudet, A. L.; O'Brien, W. E. Mammalian urea cycle enzymes. *Annual review of genetics* **1986**, *20*, 431−464.

(5) Wu, G.; Bazer, F. W.; Davis, T. A.; Kim, S. W.; Li, P.; Marc Rhoads, J.; Carey Satterfield, M.; Smith, S. B.; Spencer, T. E.; Yin, Y. Arginine metabolism and nutrition in growth, health and disease. *Amino acids* **2009**, *37* (1), 153−168.

(6) Marletta, M. A.; Yoon, P. S.; Iyengar, R.; Leaf, C. D.; Wishnok, J. S. Macrophage oxidation of L-arginine to nitrite and nitrate: nitric oxide is an intermediate. *Biochemistry* **1988**, *27* (24), 8706−8711.

(7) Palmer, R. M. J.; Ashton, D. S.; Moncada, S. Vascular endothelial cells synthesize nitric oxide from L-arginine. *Nature* **1988**, *333* (6174), 664−666.

(8) Bredt, D. S.; Snyder, S. H. Nitric oxide: a physiologic messenger molecule. *Annual review of biochemistry* **1994**, *63* (1), 175−195.

(9) Moncada, S.; Higgs, E. A. Molecular mechanisms and therapeutic strategies related to nitric oxide. *FASEB J.* **1995**, *9* (13), 1319−1330.

(10) Kossel, A.; Dakin, H. D. *Über die Arginase*, 1904.

(11) Krebs, H. A.; Henseleit, K. *Hoppe-Seyler's Zeitschrift für Physiologische Chemie*, 1932.

(12) Morris, S. M., Jr. Regulation of enzymes of the urea cycle and arginine metabolism. *Annual review of nutrition* **2002**, *22*, 87−105.

(13) Wyss, M.; Kaddurah-Daouk, R. Creatine and Creatinine Metabolism. *Physiol. Rev.* **2000**, *80* (3), 1107−1213. (accessed 2024-01-17).

(14) Foster, G. L.; Schoenheimer, R.; Rittenberg, D. Studies in protein metabolism: V. The utilization of ammonia for amino acid and creatine formation in animals. *J. Biol. Chem.* **1939**, *127* (1), 319−327.

(15) Rehberg, P. B. Studies on kidney function: the rate of filtration and reabsorption in the human kidney. *Biochem. J.* **1926**, *20* (3), 447.

(16) Calabrò, R. S.; Gervasi, G.; Bramanti, P. L-Arginine and vascular diseases: lights and pitfalls! *Acta Bio-med.: Atenei Parmensis* **2014**, *85* (3), 222−228.

(17) Schlune, A.; Vom Dahl, S.; Häussinger, D.; Ensenauer, R.; Mayatepek, E. Hyperargininemia due to arginase I deficiency: the original patients and their natural history, and a review of the literature. *Amino acids* **2015**, *47* (9), 1751−1762.

(18) Klotz, T.; Mathers, M. J.; Braun, M.; Bloch, W.; Engelmann, U. Effectiveness of Oral L-Arginine in First-Line Treatment of Erectile Dysfunction in a Controlled Crossover Study. *Urologia Internationalis* **2000**, *63* (4), 220−223. (accessed 2024-01-19).

(19) Kobori, Y.; Suzuki, K.; Iwahata, T.; Shin, T.; Sadaoka, Y.; Sato, R.; Nishio, K.; Yagi, H.; Arai, G.; Soh, S.; et al. Improvement of seminal quality and sexual function of men with oligoasthenoteratozoospermia syndrome following supplementation with L-arginine and Pycnogenol®. *Archivio Italiano di Urologia e Andrologia* **2015**, *87* (3), 190−193. (accessed 2024-01-19).

(20) Gokce, N. L-Arginine and Hypertension. *Journal of Nutrition* **2004**, *134* (10), 2807S−2811S.

(21) Drohomirecka, A.; Waś, J.; Wiligórska, N.; Rywik, T. M.; Komuda, K.; Sokołowska, D.; Lutyńska, A.; Zieliński, T. L-arginine and Its Derivatives Correlate with Exercise Capacity in Patients with Advanced Heart Failure. *Biomolecules* **2023**, *13* (3), 423.

(22) Vettore, L.; Westbrook, R. L.; Tennant, D. A. New aspects of amino acid metabolism in cancer. *British journal of cancer* **2020**, *122* (2), 150−156.

(23) Lieu, E. L.; Nguyen, T.; Rhyne, S.; Kim, J. Amino acids in cancer. *Experimental & molecular medicine* **2020**, *52* (1), 15−30.

(24) Cormerais, Y.; Vucetic, M.; Pouysségur, J. Targeting amino acids transporters (SLCs) to starve cancer cells to death. *Biochemical and biophysical research communications* **2019**, *520* (4), 691−693.

(25) Ma, Q.; Wang, Z.; Zhang, M.; Hu, H.; Li, J.; Zhang, D.; Guo, K.; Sha, H. Targeting the L-arginine-nitric oxide pathway for cancer treatment. *Current pharmaceutical design* **2010**, *16* (4), 392−410.

(26) Lind, D. S. Arginine and cancer. *J. Nutr.* **2004**, *134* (10), 2837S−2841S.

(27) Chen, C. L.; Hsu, S. C.; Ann, D. K.; Yen, Y.; Kung, H. J. Arginine Signaling and Cancer Metabolism. *Cancers* **2021**, *13* (14), 3541.

(28) Qiu, F.; Chen, Y. R.; Liu, X.; Chu, C. Y.; Shen, L. J.; Xu, J.; Gaur, S.; Forman, H. J.; Zhang, H.; Zheng, S.; et al. Arginine starvation impairs mitochondrial respiratory function in ASS1-deficient breast cancer cells. *Science signaling* **2014**, *7* (319), ra31.

(29) Chan, P. Y.; Phillips, M. M.; Ellis, S.; Johnston, A.; Feng, X.; Arora, A.; Hay, G.; Cohen, V. M. L.; Sagoo, M. S.; Bomalaski, J. S.; et al. A Phase 1 study of ADI-PEG20 (pegargiminase) combined with cisplatin and pemetrexed in ASS1-negative metastatic uveal melanoma. *Pigment cell & melanoma research* **2022**, *35* (4), 461−470.

(30) Ensor, C. M.; Holtsberg, F. W.; Bomalaski, J. S.; Clark, M. A. Pegylated arginine deiminase (ADI-SS PEG20,000 mw) inhibits human melanomas and hepatocellular carcinomas in vitro and in vivo. *Cancer Res.* **2002**, *62* (19), 5443−5450.

(31) De Santo, C.; Booth, S.; Vardon, A.; Cousins, A.; Tubb, V.; Perry, T.; Noyvert, B.; Beggs, A.; Ng, M.; Halsey, C.; et al. The arginine metabolome in acute lymphoblastic leukemia can be targeted by the pegylated-recombinant arginase I BCT-100. *International journal of cancer* **2018**, *142* (7), 1490−1502.

(32) Mussai, F.; Egan, S.; Higginbotham-Jones, J.; Perry, T.; Beggs, A.; Odintsova, E.; Loke, J.; Pratt, G.; U, K. P.; Lo, A.; et al. Arginine dependence of acute myeloid leukemia blast proliferation: a novel therapeutic target. *Blood* **2015**, *125* (15), 2386−2396.

(33) Delage, B.; Fennell, D. A.; Nicholson, L.; McNeish, I.; Lemoine, N. R.; Crook, T.; Szlosarek, P. W. Arginine deprivation and argininosuccinate synthetase expression in the treatment of cancer. *International journal of cancer* **2010**, *126* (12), 2762−2772.

(34) Cheng, C. T.; Qi, Y.; Wang, Y. C.; Chi, K. K.; Chung, Y.; Ouyang, C.; Chen, Y. R.; Oh, M. E.; Sheng, X.; Tang, Y.; et al.

Arginine starvation kills tumor cells through aspartate exhaustion and mitochondrial dysfunction. *Commun. Biol.* **2018**, *1*, 178.
(35) Tsai, H. J.; Jiang, S. S.; Hung, W. C.; Borthakur, G.; Lin, S. F.; Pemmaraju, N.; Jabbour, E.; Bomalaski, J. S.; Chen, Y. P.; Hsiao, H. H.; et al. A Phase II Study of Arginine Deiminase (ADI-PEG20) in Relapsed/Refractory or Poor-Risk Acute Myeloid Leukemia Patients. *Sci. Rep.* **2017**, *7* (1), 11253.
(36) Siaghy, E. M.; Devaux, Y.; Schroeder, H.; Sfaksi, N.; Ungureanu-Longrois, D.; Zannad, F.; Villemot, J. P.; Nabet, P.; Mertes, P. M. High-performance liquid chromatographic analysis of muscular interstitial arginine and norepinephrine kinetics. A microdialysis study in rats. *Journal of chromatography. B, Biomedical sciences and applications* **2000**, *745* (2), 279−286.
(37) Watts, J.; Fowler, L.; Whitton, P. S.; Pearce, B. Release of arginine, glutamate and glutamine in the hippocampus of freely moving rats: Involvement of nitric oxide. *Brain research bulletin* **2005**, *65* (6), 521−528.
(38) Seim, G. L.; Britt, E. C.; Fan, J. Analysis of Arginine Metabolism Using LC-MS and Isotopic Labeling. *Methods in molecular biology (Clifton, N.J.)* **2019**, *1978*, 199−217.
(39) Bogner, M.; Ludewig, U. Visualization of arginine influx into plant cells using a specific FRET-sensor. *J. Fluoresc* **2007**, *17* (4), 350−360.
(40) Okada, S.; Ota, K.; Ito, T. Circular permutation of ligand-binding module improves dynamic range of genetically encoded FRET-based nanosensor. *Protein Sci.* **2009**, *18* (12), 2518−2527.
(41) Whitfield, J. H.; Zhang, W. H.; Herde, M. K.; Clifton, B. E.; Radziejewski, J.; Janovjak, H.; Henneberger, C.; Jackson, C. J. Construction of a robust and sensitive arginine biosensor through ancestral protein reconstruction. *Protein science: a publication of the Protein Society* **2015**, *24* (9), 1412−1422.
(42) Lüneburg, N.; Xanthakis, V.; Schwedhelm, E.; Sullivan, L. M.; Maas, R.; Anderssohn, M.; Riederer, U.; Glazer, N. L.; Vasan, R. S.; Böger, R. H. Reference intervals for plasma L-arginine and the L-arginine:asymmetric dimethylarginine ratio in the Framingham Offspring Cohort. *J. Nutr.* **2011**, *141* (12), 2186−2190.
(43) Mao, Y.; Shi, D.; Li, G.; Jiang, P. Citrulline depletion by ASS1 is required for proinflammatory macrophage activation and immune responses. *Mol. Cell* **2022**, *82* (3), 527−541.E7.
(44) Rosen, B. P. Basic amino acid transport in Escherichia coli: properties of canavanine-resistant mutants. *J. Bacteriol.* **1973**, *116* (2), 627−635.
(45) Vahedi-Faridi, A.; Eckey, V.; Scheffel, F.; Alings, C.; Landmesser, H.; Schneider, E.; Saenger, W. Crystal structures and mutational analysis of the arginine-, lysine-, histidine-binding protein ArtJ from Geobacillus stearothermophilus. Implications for interactions of ArtJ with its cognate ATP-binding cassette transporter, Art(MP)2. *Journal of molecular biology* **2008**, *375* (2), 448−459.
(46) Soriani, M.; Petit, P.; Grifantini, R.; Petracca, R.; Gancitano, G.; Frigimelica, E.; Nardelli, F.; Garcia, C.; Spinelli, S.; Scarabelli, G.; et al. Exploiting antigenic diversity for vaccine design: the chlamydia ArtJ paradigm. *J. Biol. Chem.* **2010**, *285* (39), 30126−30138.
(47) Marvin, J. S.; Borghuis, B. G.; Tian, L.; Cichon, J.; Harnett, M. T.; Akerboom, J.; Gordus, A.; Renninger, S. L.; Chen, T. W.; Bargmann, C. I.; et al. An optimized fluorescent probe for visualizing glutamate neurotransmission. *Nat. Methods* **2013**, *10* (2), 162−170.
(48) Marvin, J. S.; Schreiter, E. R.; Echevarría, I. M.; Looger, L. L. A genetically encoded, high-signal-to-noise maltose sensor. *Proteins* **2011**, *79* (11), 3025−3036.
(49) Aggarwal, A.; Liu, R.; Chen, Y.; Ralowicz, A. J.; Bergerson, S. J.; Tomaska, F.; Mohar, B.; Hanson, T. L.; Hasseman, J. P.; Reep, D.; et al. Glutamate indicators with improved activation kinetics and localization for imaging synaptic transmission. *Nat. Methods* **2023**, *20* (6), 925−934.
(50) Marvin, J. S.; Shimoda, Y.; Magloire, V.; Leite, M.; Kawashima, T.; Jensen, T. P.; Kolb, I.; Knott, E. L.; Novak, O.; Podgorski, K.; et al. A genetically encoded fluorescent sensor for in vivo imaging of GABA. *Nat. Methods* **2019**, *16* (8), 763−770.
(51) Sun, F.; Zhou, J.; Dai, B.; Qian, T.; Zeng, J.; Li, X.; Zhuo, Y.; Zhang, Y.; Wang, Y.; Qian, C.; et al. Next-generation GRAB sensors for monitoring dopaminergic activity in vivo. *Nat. Methods* **2020**, *17* (11), 1156−1166.
(52) Kang, C. H.; Kim, S. H.; Nikaido, K.; Gokcen, S.; Ames, G. F. Crystallization and preliminary X-ray studies of HisJ and LAO periplasmic proteins from Salmonella typhimurium. *J. Mol. Biol.* **1989**, *207* (3), 643−644.
(53) Kang, C. H.; Shin, W. C.; Yamagata, Y.; Gokcen, S.; Ames, G. F.; Kim, S. H. Crystal structure of the lysine-, arginine-, ornithine-binding protein (LAO) from Salmonella typhimurium at 2.7-A resolution. *J. Biol. Chem.* **1991**, *266* (35), 23893−23899.
(54) Nikaido, K.; Ames, G. F. Purification and characterization of the periplasmic lysine-, arginine-, ornithine-binding protein (LAO) from Salmonella typhimurium. *J. Biol. Chem.* **1992**, *267* (29), 20706−20712.
(55) Oh, B. H.; Pandit, J.; Kang, C. H.; Nikaido, K.; Gokcen, S.; Ames, G. F.; Kim, S. H. Three-dimensional structures of the periplasmic lysine/arginine/ornithine-binding protein with and without a ligand. *J. Biol. Chem.* **1993**, *268* (15), 11348−11355.
(56) Oh, B. H.; Ames, G. F.; Kim, S. H. Structural basis for multiple ligand specificity of the periplasmic lysine-, arginine-, ornithine-binding protein. *J. Biol. Chem.* **1994**, *269* (42), 26323−26330.
(57) Unger, E. K.; Keller, J. P.; Altermatt, M.; Liang, R.; Matsui, A.; Dong, C.; Hon, O. J.; Yao, Z.; Sun, J.; Banala, S.; et al. Directed Evolution of a Selective and Sensitive Serotonin Sensor via Machine Learning. *Cell* **2020**, *183* (7), 1986−2002.E26.
(58) Afshinpour, M.; Mahdiuni, H. Arginine transportation mechanism through cationic amino acid transporter 1: insights from molecular dynamics studies. *J. Biomol. Struct. Dyn.* **2023**, *41* (23), 13580−13594.
(59) Banjarnahor, S.; Rodionov, R. N.; König, J.; Maas, R. Transport of L-Arginine Related Cardiovascular Risk Markers. *J. Clin. Med.* **2020**, *9* (12), 3975.
(60) Van Zandt, M. C.; Whitehouse, D. L.; Golebiowski, A.; Ji, M. K.; Zhang, M.; Beckett, R. P.; Jagdmann, G. E.; Ryder, T. R.; Sheeler, R.; Andreoli, M.; et al. Discovery of (R)-2-amino-6-borono-2-(2-(piperidin-1-yl)ethyl)hexanoic acid and congeners as highly potent inhibitors of human arginases I and II for treatment of myocardial reperfusion injury. *J. Med. Chem.* **2013**, *56* (6), 2568−2580.
(61) Cheng, J.; Valdivia, C. R.; Vaidyanathan, R.; Balijepalli, R. C.; Ackerman, M. J.; Makielski, J. C. Caveolin-3 suppresses late sodium current by inhibiting nNOS-dependent S-nitrosylation of SCN5A. *J. Mol. Cell Cardiol* **2013**, *61*, 102−110.
(62) Zhang, S.; Liu, Y.; Zhou, X.; Ou, M.; Xiao, G.; Li, F.; Wang, Z.; Wang, Z.; Liu, L.; Zhang, G. Sirtuin 7 Regulates Nitric Oxide Production and Apoptosis to Promote Mycobacterial Clearance in Macrophages. *Front Immunol* **2021**, *12*, No. 779235.
(63) Nakamura, T.; Prewitt, R. L. Effect of NG-monomethyl-L-arginine on arcade arterioles of rat spinotrapezius muscles. *Am. J. Physiol.: Heart Cirul. Physiol.* **1991**, *261* (1), H46−H52.
(64) Maggi, C. A.; Barbanti, G.; Turini, D.; Giuliani, S. Effect of NG-monomethyl L-arginine (L-NMMA) and NG-nitro L-arginine (L-NOARG) on non-adrenergic non-cholinergic relaxation in the circular muscle of the human ileum. *Br. J. Pharmacol.* **1991**, *103* (4), 1970−1972.
(65) Frey, C.; Narayanan, K.; McMillan, K.; Spack, L.; Gross, S. S.; Masters, B. S.; Griffith, O. W. L-thiocitrulline. A stereospecific, heme-binding inhibitor of nitric-oxide synthases. *J. Biol. Chem.* **1994**, *269* (42), 26083−26091.
(66) Zhang, J. F.; Liu, B.; Hong, I.; Mo, A.; Roth, R. H.; Tenner, B.; Lin, W.; Zhang, J. Z.; Molina, R. S.; Drobizhev, M.; et al. An ultrasensitive biosensor for high-resolution kinase activity imaging in awake mice. *Nat. Chem. Biol.* **2021**, *17* (1), 39−46.
(67) Aryal, S. P.; Xia, M.; Adindu, E.; Davis, C.; Ortinski, P. I.; Richards, C. I. ER-GCaMP6f: An Endoplasmic Reticulum-Targeted Genetic Probe to Measure Calcium Activity in Astrocytic Processes. *Anal. Chem.* **2022**, *94* (4), 2099−2108.

https://doi.org/10.1021/acssensors.4c03174
ACS Sens. XXXX, XXX, XXX−XXX

(68) Schmitt, D. L.; Curtis, S. D.; Lyons, A. C.; Zhang, J. F.; Chen, M.; He, C. Y.; Mehta, S.; Shaw, R. J.; Zhang, J. Spatial regulation of AMPK signaling revealed by a sensitive kinase activity reporter. *Nat. Commun.* **2022**, *13* (1), 3856.
(69) Chen, M.; Sun, T.; Zhong, Y.; Zhou, X.; Zhang, J. A Highly Sensitive Fluorescent Akt Biosensor Reveals Lysosome-Selective Regulation of Lipid Second Messengers and Kinase Activity. *ACS Central Science* **2021**, *7* (12), 2009−2020.
(70) Cheng, C.-T.; Qi, Y.; Wang, Y.-C.; Chi, K. K.; Chung, Y.; Ouyang, C.; Chen, Y.-R.; Oh, M. E.; Sheng, X.; Tang, Y.; et al. Arginine starvation kills tumor cells through aspartate exhaustion and mitochondrial dysfunction. *Communications Biology* **2018**, *1* (1), 178.
(71) Li, R.; Li, Y.; Jiang, K.; Zhang, L.; Li, T.; Zhao, A.; Zhang, Z.; Xia, Y.; Ge, K.; Chen, Y. Lighting up arginine metabolism reveals its functional diversity in physiology and pathology. *Cell Metabolism* **2025**, *37* (1), 291−304.E9.
(72) Marvin, J. S.; Scholl, B.; Wilson, D. E.; Podgorski, K.; Kazemipour, A.; Müller, J. A.; Schoch, S.; Quiroz, F. J. U.; Rebola, N.; Bao, H.; et al. Stability, affinity, and chromatic variants of the glutamate sensor iGluSnFR. *Nat. Methods* **2018**, *15* (11), 936−939.

https://doi.org/10.1021/acssensors.4c03174
ACS Sens. XXXX, XXX, XXX−XXX